How to Cite:
Dandagvhal, K., & Chatpalliwar, V. (2022). In silico Characterization, ADMET prediction and Molecular Docking studies of few 2/3 carboxylate-4/5/6-monosubstitued indole derivatives as potential GSK-3β inhibitors. *International Journal of Health Sciences*, *6*(S3), 12193–12212. https://doi.org/10.53730/ijhs.v6nS3.9119

In silico Characterization, ADMET prediction and Molecular Docking studies of few 2/3 carboxylate-4/5/6-monosubstitued indole derivatives as potential GSK-3β inhibitors

Kamlesh Dandagvhal
Research Scholar, Shriman Sureshdada Jain College of Pharmacy, Chandwad, Nashik, India
*Corresponding author email: kamleshdndgvhl16@gmail.com

Vivekanand Chatpalliwar
Professor and Head, Department of Pharmaceutical Chemistry, Shriman Sureshdada Jain College of Pharmacy, Chandwad, Nashik, India

***Abstract*---**Diabetes Mellitus is a leading cause of high mortality rate in the world. Recently, GSK-3β inhibitors showed promising results to treat Diabetes mellitus and several such molecules are in clinical trials. Ethyl 2/3-carboxylate-4/5/6-monosubstituted-1H-indole derivatives were designed with the aim to search new lead molecules. The molecular structures were drawn in ChemBiodraw Ultra© and molecular docking studies were performed by using Schrödinger and AutoDock 1.5.6 software. Few in silico properties such as Log P and toxicity profile were predicted online using SwissADME and PreADMET respectively. Amongst all the designed molecules, few derivatives showed maximum binding affinity in LBD of 6V6L protein. The lipophilic character of the molecules was predicted through their individual Log P Values; molecules with better binding affinities in LBD displayed Log P values of 2.25-3.13. Additionally, some of the designed molecules were subjected to PreADMET for predicting their safety and few were predicted to induce toxic reaction were as others were predicted to be safe in the models that were selected for prediction. Ethyl 2/3-carboxylate-4/5/6-monosubstituted-1H-indole derivative were designed resulting in new molecules with high binding affinities, also few of these molecules were predicted to be non-carcinogenic with low Log P values.

***Keywords*---**GSK-3β, Diabetes mellitus, Indole, docking, ADMET.

Introduction

Protein phosphorylation and dephosphorylation are significant processes in the regulation of protein functions. Protein kinases catalyze biological phosphorylations -the number of which in the human genome exceeds 500- which happens mostly with hydroxylated amino acids such as serine, threonine, and tyrosine. The significance of protein phosphorylation as a primary regulatory mechanism used by cells to monitor enzymes and other proteins and the association of many diseases with their aberrations[1] render kinases as important targets and, in recent years, the search for kinase inhibitors has rekindled much interest by scientific community of drug design programmes. *Glycogen synthase kinase-3* (*GSK-3*) was identified as a rate determining enzyme in glycogen biosynthesis as a regulator of *glycogen synthase* (*GS*) [2-4]. The aforementioned is a cytosolic serine/threonine kinase that has been identified to exist in two isoforms (α & β) in the mammals. It has several substrates [5, 6] and plays critical roles in glucose homeostasis[7], CNS functions, and predisposition of cancer[8], circadian rhythm, cell survival & apoptosis. These isoforms share high homology (≥ 95 %) at the catalytic domain and are ubiquitously expressed in cellular systems having similar biochemical properties.

GSK-3β inactivates *GS* by phosphorylation, inhibiting the synthesis of glycogen. A signalling cascade clues to the triggering of *GSK-3β* following the interaction of insulin with its receptor in the plasma membranes, which in turn deactivates *GSK-3β* through phosphorylating the tyrosine-hydroxyl (Tyr 216). *GS* in the cellular environment remains active and hence, glycogen synthesis remains stimulated. Inhibition of *GSK-3β* by small molecule kinase inhibitors, therefore, has been considered as a helpful strategy for treating diabetes. *GSK-3* inhibitors have a broad spectrum of therapeutic potential, among which diabetes, neurodegenerative diseases[9], bipolar disorders[10], stroke, cancer, and chronic inflammatory diseases are the major ailments, based on the role of phosphorylation and different substrates that these kinases targets in cellular and physiological events. A number of *GSK-3* inhibitors have been identified, including hymenialdisines[10], paullones[11], indirubins[12], and derivatives of maleimide (bisarylmaleimides[13], anilinomaleimides[14], bisindolylmaleimides[15], azaindolyl maleimides[16]). Despite the chemical diversity and their enormous potential for *GSK-3β* inhibition, there is no drug operating through this strategy.

Promising inhibitory effects against *GSK-3β* are witnessed in several naturally existing molecule with complex chemistry but have one characteristic heterocyclic nucleus as a common factor, *i. e.* the 1*H*-indole, hence, the current research focuses on designing indole derivatives, evaluating their potential to bind with the virtual enzyme in its LBD, synthesizing selected derivatives and evaluating their *GSK-3β* inhibiting potential through *in vitro* assay. The utility of the synthesized molecules as therapeutically useful entities depends on few characteristic properties known as 'drug-likeness'.[17] Before synthesis, it becomes imperative to predict the bioavailability and bioavailability-related features like solubility and lipophilicity of the designed molecules. This possibly avoids energy, resources and time going down the drain. Hence, *in silico* ADME prediction and toxicity profiling through *SwissADME* and *PreADMET*, respectively, was studied for all designed molecules. Accordingly, the designed molecules were studied for checking their

alignment with *The Lipinski Rule of Five* and ADMET study for drug-likeness. Several co-crystalized proteins available on RCSB-PDB representing *GSK-3β* were subjected to checking resolution and virtual quality through *Ramchandran plot* [18, 19] before using for docking analyses of the designed molecules. Those molecules showing suitable interactions and acceptable *G score* in the docking analysis were selected for laboratory synthesis and further evaluations.

Materials and Methods

Co-crystal of *GSK-3β* (PDB ID: 5K5N, 5KPK, 5F94, 6V6L, 6GN1, 9Y9R) were obtained from the RCSB Protein Data Bank (http://www.rcsb.org/pdb/home/home.do). Virtual indole derivatives (ligands) were constructed using *CS ChemDraw Ultra 8.0* for docking analysis (Table No. 1). *Schrödinger 2020* and *Auto Dock Tools (ADT) (version 1.5.7)* were used for molecular docking studies and *Discovery Studio 2021* for studying the interactions of ligands within LBD of the protein (Figure No. 1) in detail[20]. ADME studies were carried virtually in *SwissADME* and toxicity profiling using *PreADMET* (https://preadmet.webservice.bmdrc.org/toxicity/)

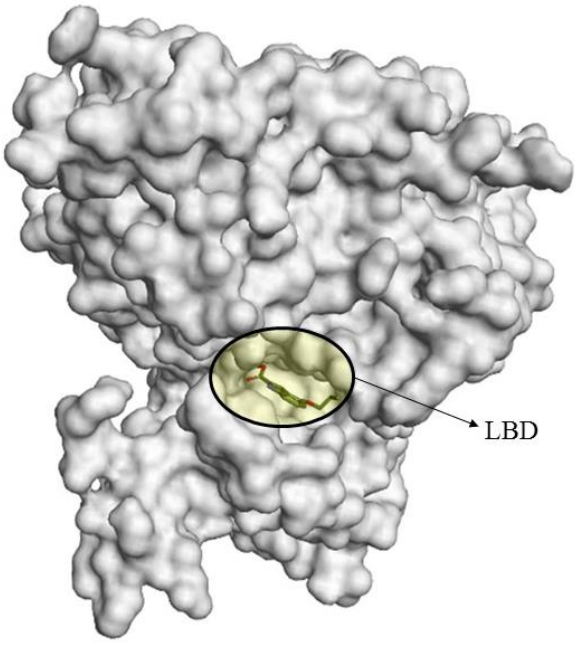

Figure 1. Active site located deep inside the LBD (shaded portion) of *GSK-3β*

Ramachandran plot

Co-crystal of *GSK-3β* (PDB ID: 5K5N, 5KPK, 5F94, 6V6L, 6GN1, 9Y9R) were obtained from the RCSB-PDB in *.*pdb* format. These files were uploaded to the *Ram plot server* (https://zlab.umassmed.edu/bu/rama/) to obtain their respective *Ramachandran plots,* and are presented in Figure No. 2 and statistical observation are presented in Table No. 2.

The *G factor* is a measure of appropriateness of a co-crystalized protein considering its stereo-chemical feature. A low *G factor* suggests that a feature corresponds to a low-probability conformation when applied to a specific residue. As a result, residues that appear in the disallowed regions have a low (or very negative) *G factor*. Unfavorable *chi1-chi2* and *chi1* values behave similarly. Low *G factor* for a protein indicates inappropriate conformations, whereas, *R factor* is a measure of the agreement between the crystallographic model and the experimental X-ray diffraction data. In a good protein structure, the difference between *R-factor* and *Free R-factor* should be less than 5%. The data so obtained is presented Table No. 02 for comparative assessment.

Molecular docking

Glide XP docking was performed aimed to calculate the binding affinities of native co-crystallized ligands originally available with respected to proteins along with virtual indole derivatives using *Prime/MM-GBSA* module, and the binding scores are expressed in kcal/mol which are listed in Table No. 3, these were compared for deciding the better interacting ligands. Further docking studies were performed using the *ADT* to fathom the ligand interactions with the protein. Ligand were virtually prepared by adding *Gasteiger charges*. Other attributes as redundant chains, non-essential ions, water molecules, and native ligands were discarded. The *PDBQT* formats of ligands and the protein, 6V6L, were prepared by the *ADT 1.5.4* package (http://mgltools.scripps.edu).[21]

Conformations of binding ligands were studied by setting torsions of the ligands and detecting the roots. *Genetic algorithm* was set as a search parameter[22]. Number of search for genetic algorithm was set to 30 and population size was kept at 300. Grid was prepared having 0.47 Å radius in the active site, with X center: 2.497444, Y center: 0.167722 and Z center: -17.404583, with dimensions of 60° each, within which all atoms of the native ligand [(23)] were accommodated in the LBD. The standard ligand and all designed ligands were docked into the crystal structure of the enzyme to validate the molecular docking procedure, setting root mean square deviation (RMSD) at 2.0 tolerance. The remaining parameters, *viz.* random number generator, energy parameter, step size parameter *etc.* were set as default. Binding energies for different complexes obtained were used for the initial evaluation of result. A cluster analysis based on RMSD values was further performed to find the lowest energy conformation and it was selected as the most reliable solution. For each docking run, top ten most suitable docking poses were saved for further studies.

ADME analysis

It has been recommended that the employment of computational ADME, in combination with *in vivo* and *in vitro* predictions, should be studied as early as possible in the drug discovery process so as to reduce the number of safety issues[24]. *Lipinski's rule of five* is useful for summarizing a drug candidate's molecular characteristics and is useful in the development of a prospective therapeutic molecule. [25, 26] For this experiment, the ADME study was conducted utilizing the *SwissADME* predictor to evaluate the ADMET properties, like aqueous solubility (Log *S*), skin permeability (Log *Kp*), synthetic accessibility score

(SA), percentage absorption, pharmacokinetics, drug-likeness, and medicinal chemistry openness properties of designed molecules.[27] The criteria of molecular weight ≤ 500, ≤ 5 hydrogen-bond donors (HBD), 10≤ hydrogen-bond acceptors (HBA), and ≤10 rotatable bonds (RB) stood designated for the present study.[28] The combined findings from multiple Log *P* and *S* prediction tools such as ILOGP, XLOGP3, WLOGP, ESOL, and SILICOS-IT to get a comprehensive result on lipophilicity and hydrophilicity of designed molecules. In this study, prediction and significant descriptors of druglikeness such as mutagenicity, toxicological dosage level for different tissues and pharmacologically relevant properties of the compounds were predicted and presented in Table No. 6 using *PreADMET* server. (http://preadmet.bmdrc.org/)

Results and Discussion

Substituted indole derivatives were designed to retain structural features that appeared in relevant literature [29-32] and were reported to interact with amino acid residues in LBD of *GSK-3β*, with few substitutions being incorporated logically, and the structures are given in Table No. 1

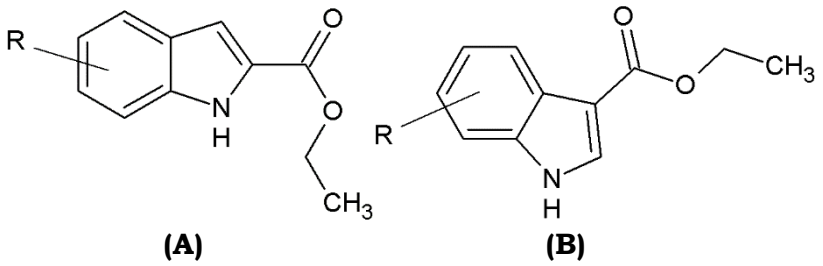

Table 1
Ethyl 2/3-carboxylate-4/5/6-monosubstituted-1H-indole derivatives

Ligand Code	Position	R
Ai1-Ai113 Bi1-Bi113	4	1. - Cl, 2. – Br, 3. –F, 4. –I, 5. $–NH_2$ 6.-OCH_3 7.-NO_2, 8. – CH_3, 9. – OCH_3, 10. – OC_2H_5, 11. – OC_3H_7 12. – isopropyl, 13.- isopropoxy, 14. – C_2H_5 15. – C_3H_7 16. – C_4H_9 17. – C_5H_{11}, 18. – CH_2OH, 19. – C_2H_4OH 20. – C_3H_6OH, 21. – C_4H_8OH, 22. – $C_5H_{10}OH$, 23. – CH_2OHCH_3, 24. – $CH_2OHC_2H_5$, 25. – $CH_2OHC_3H_7$, 26. – $CH_2OHC_4H_9$, 27. – $CH_2CHOHCH_3$ 28. – $CH_2CHOHC_2H_5$, 29. – $CH_2CHOHC_3H_7$, 30. – CH_2Cl, 31. – C_2H_4OH, 32. – C_3H_6OH, 33. – C_4H_8OH, 34. – $C_5H_{10}OH$, 35. – CH_2OHCH_3, 36. – $CH_2OHC_2H_5$, 37. – $CH_2OHC_3H_7$, 38. – $CH_2OHC_4H_9$, 39. – $CH_2CHOHCH_3$, 40. – $CH_2CHOHC_2H_5$, 41.- $CH_2CHOHC_3H_7$, 42.- CH_2Br, 43. – C_2H_4OH, 44. – C_3H_6OH, 45. – C_4H_8OH, 46. - $C_5H_{10}OH$ 47. – CH_2OHCH_3, 48. – $CH_2OHC_2H_5$, 49. – $CH_2OHC_3H_7$ 50. – $CH_2OHC_4H_9$, 51. – $CH_2CHOHCH_3$, 52. – $CH_2CHOHC_2H_5$, 53. – $CH_2CHOHC_3H_7$, 54. – CH_2F, 55. – C_2H_4OH, 56. – C_3H_6OH, 57. – C_4H_8OH, 58. – $C_5H_{10}OH$, 59. – CH_2OHCH_3, 60. – $CH_2OHC_2H_5$, 61. – $CH_2OHC_3H_7$, 62. –$CH_2OHC_4H_9$ 63. – $CH_2CHOHCH_3$, 64. – $CH_2CHOHC_2H_5$, 65. – $CH_2CHOHC_3H_7$, 66. – CH_2I, 67. – C_2H_4OH, 68. – C_3H_6OH, 69. –C_4H_8OH, 70. –$C_5H_{10}OH$, 71. – CH_2OHCH_3, 72. – $CH_2OHC_2H_5$, 73. – $CH_2OHC_3H_7$, 74. – $CH_2OHC_4H_9$, 75. –
Aii1-Aii113 Bii1-Bii113	5	
Aiii1-Aiii113 Biii1-Biii113	6	
Aiv1-Aiii113 Biv1-Biv113	7	

		$CH_2CHOHCH_3$, 76. – $CH_2CHOHC_2H_5$, 77. –$CH_2CHOHC_3H_7$, 78. – CH_2NH_2, 79. – C_2H_4OH, 80. – C_3H_6OH, 81.-C_4H_8OH, 82. – $C_5H_{10}OH$, 83. – CH_2OHCH_3, 84. – $CH_2OHC_2H_5$, 85. – $CH_2OHC_3H_7$, 86. – $CH_2OHC_4H_9$, 87. – $CH_2CHOHCH_3$, 88. – $CH_2CHOHC_2H_5$ 89. – $CH_2CHOHC_3H_7$, 90. – $CH_2NHCOCH_3$, 91. – C_2H_4OH, 92. – C_3H_6OH, 93. – C_4H_8OH, 94. – $C_5H_{10}OH$, 95.- CH_2OHCH_3, 96. - $CH_2OHC_2H_5$, 97. – $CH_2OHC_3H_7$, 98. – $CH_2OHC_4H_9$, 99. – $CH_2CHOHCH_3$, 100. – $CH_2CHOHC_2H_5$, 101. – $CH_2CHOHC_3H_7$, 102. – CH_2NO_2, 103. – C_2H_4OH, 104. – C_3H_6OH, 105. – C_4H_8OH, 106. – $C_5H_{10}OH$, 107. – CH_2OHCH_3, 108. – $CH_2OHC_2H_5$, 109. – $CH_2OHC_3H_7$, 110. – $CH_2OHC_4H_9$, 111. – $CH_2CHOHCH_3$, 112. – $CH_2CHOHC_2H_5$, 113. – $CH_2CHOHC_3H_7$

The crystal structure of *GSK-3β* profoundly appearing in the relevant literature[29-32], precisely 6, were subjected to resolution and to quality analysis using *Ramachandran plot*, and the obtained results are presented in Table No. 2. In the plot shown below, blue dots represent amino acid residue and peptide linkage whereas the red region represent the interstitial spaces present in LBD. The brown and yellow colour represent the other portions of the proteins. Co-crystal 6V6L and 6Y9R display favourable conformations of amino acid residues whereby their side chains accommodate the docking ligands. However, unfavourable geometry of amino acid residues have been displayed by showing wide scatter of amino acid residues in the disallowed region shown in white.

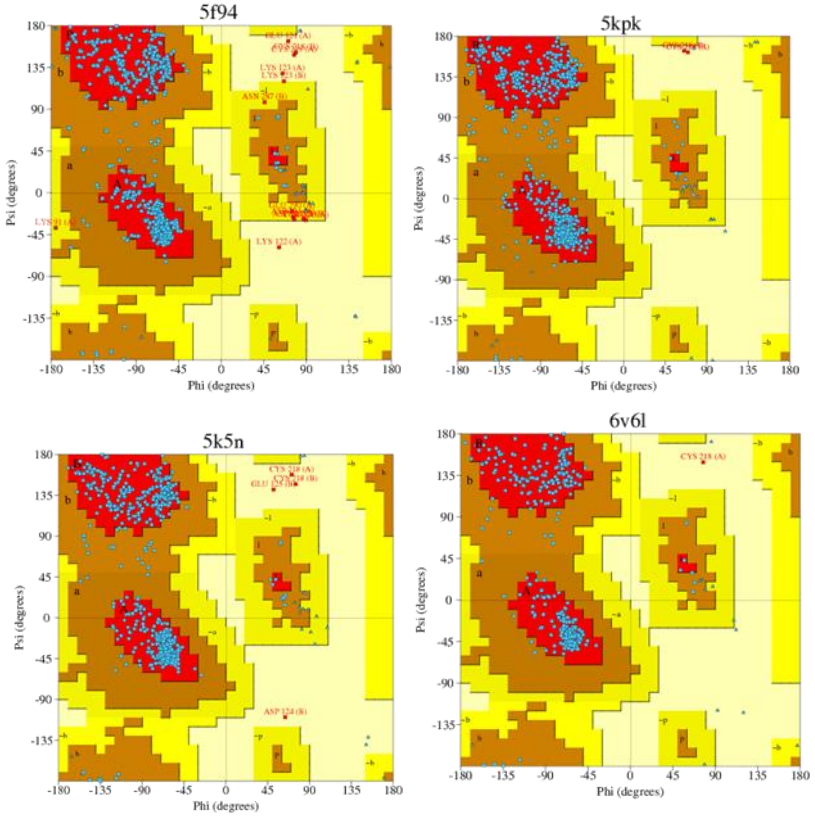

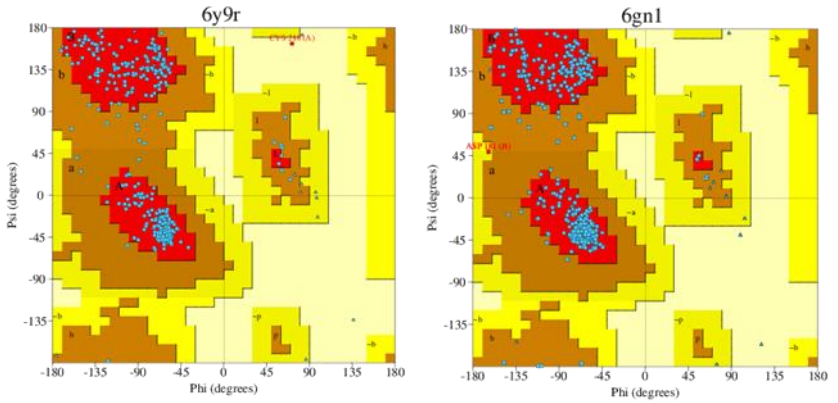

Figure 2. *Ramachandra plot* of crystal structures -6Y9R, 6V6L, 6GN1, 5F94, 5K5N, 5KPK- of *GSK-3β*

Table 2
Statistics of Ramachandran Plot study of six co-crystallized structures representing GSK-3β

Protein *GSK-3β*	Resolution (Å)	*R-factor*	*R-free*	Total number of residues	Percent of Most favoured regions [A, B, L]	Percent of disallowed regions [XX]	*G factor*s
6Y9R	2.08	0.191	0.226	350	90.5	0.3	0.16
6V6L	2.19	0.204	0.234	344	90.5	0.3	0.17
6GN1	2.60	0.224	0.259	680	91.4	0.0	0.11
5F94	2.51	0.191	0.226	695	87.4	0.1	0.13
5K5N	2.20	0.205	0.229	667	90.7	0.7	0.4
5KPK	2.40	0.170	0.224	692	87.0	0.3	-0.04

Apparently, crystal structures 6Y9R and 6V6L provided marginally better scores of resolution over others, hence these two were utilized for molecular docking of designed ligands. Ranges of *XPG score* and binding energy of designed ligands with 6Y9R and 6V6L indicate that designed ligands interact within LBD of 6V6L with better attractive forces as compared to with 6Y9R; the observations and obtained score values have been mentioned in Table No. 3, which clearly explains the selection of 6V6L for docking of designed ligands.

Table 3
Ranges of XP G Score and MM-GBSA dG bind score with respect to designed compounds

Co-crystallized *GSK-3β*	*XPG Score*	*MM-GBSA dG bind (kcal/ mol)*
6Y9R	-8.808 to -4.38	-39.51 to -21.86
6V6L	-9.143 to -4.901	-40.38 to -21.29

Molecular docking studies

Designed ligands, mentioned in Table No. 1, were docked in LBD, spanning with X center: 2.497444, Y center: 0.167722 and Z center: -17.404583 coordinates in *ADT* with dimensions of 60° each. Of the total 904 designed ligands docked in the LBD, few ligands having selective functional groups interacted favorably with the amino acid residues in LBD. Accordingly, -NO_2, -Cl, -Br, -I, -R, -OR substitutions at 4th & 5th position in indole-2-carboxylate structure were tolerated for interaction as indicated by their respective docking score, whereas the same functions on 6th and 7th position were not tolerated at all. Additionally, rest of the designed ligands did not show considerable interactions due to bulkiness of the substituent causing steric hindrance. Amino group present on side chain of LYS85 was involved in proton donor-acceptor interaction with the oxygen of nitro group present on either 4th or 5th position on indole nucleus.

Halo group function either 4th or 5th position were observed to be involved in hydrophobic interaction with side chain of LEU188 LEU132 and ALA83, and also ring-staking interaction PHE201 and TYR134. Esteric group on 2nd position of indole nucleus interacted with the peptide linkage between TYR134 and VAL135 in few of the designed ligands, whereas LYS85 was involved in interaction with same group in other ligands. The esteric oxygen accepted proton from –NH of peptide linkage of TYR134 - VAL135; and from -NH of LYS85. However the same esteric group on 3rd position of indole nucleus seemed to be less tolerated as it was devoid of any interaction. This observation strictly warrant presence of esteric group on second position rather than an alkyl chain. Docking poses of ligands are presented in Figure No

Table 4
Docking interaction of active compounds with GSK-3β in complex

Ligands	Docking score (kcal mol^{-1})	Estimated Inhibition Constant, Ki (μM)	Amino acid residues with H-bond Interaction	Amino acid residues with Hydrophobic interactions (Pi sigma, alkyl-Pi, Pi-Sulphur)
Ai1	-5.52	89.24	LYS85, ASP 200	VAL110, VAL70, MET101, LEU188, LEU132, ALA83, CYS199
Aii1	-5.77	58.63	LYS85, ASP 200	LEU188, MET101, LEU132, VAL110, TRY134, ALA83, ILE62, CYS199
Aii2	-6.39	20.73	LYS85, GLU97	MET101, PHE201, LEU132, CYS199, VAL110, LEU188, VAL70, TYR134, ALA83
Ai4	-5.75	61.07	LYS85, CYS199	VAL110, VAL70, LEU132, ILE62, MET101, LEU188, ALA83
Aii4	-6.13	31.88	LYS85	PHE201, MET101, VAL110, VAL70, LEU188, TRY134, ILE62, ALA83, LEU132, CYS199
Ai5	-6.23	27.18	LYS85	PHE67, LEU188, GLU67, ILE62, ALA83, TRY134, VAL70, CYS199
Aii5	-6.76	11.11	NH of peptide	ALA83, LEU188, VAL110,

			linkage between TYR134-VAL135 , LYS85	TYR134, ILE62, CYS199, VAL70, LEU132
Aii6	-5.53	88.37	VAL135, LYS85, TRY134, CYS199	LEU132, VAL70, ILE62, VAL110, LEU188, ALA83
Ai10	-5.31	127.56	VAL135, LYS85, CYS199	VAL110, ALA83, VAL70, LEU188, LYS85, LEU132, ASP133
Aii10	-5.84	52.75	LYS85, VAL135, CYS199, TRY134	LEU132, VAL110, ALA83, VAL70, ASP133, ILE 62, LEU188
Ai11	-5.32	125.35	LYS85, CYS199	MET101, LEU132, VAL110, VAL70, TYR134, LEU188
Aii11	-6.00	40.31	VAL135, CYS199, LYS85, ASP200, GLU97, LEU130, PHE201, TYR134	LEU188, VAL70, LEU132, MET101, ALA83, VAL110, ILE62.
Ai12	-5.67	70.38	LYS85	VAL70, ALA83, LEU188, LEU132, VAL110, CYS199, MET101
Ai13	-5.36	118.42	LYS85, CYS199	VAL70, VAL110, LEU132, MET101, LEU188, ALA83
Tideglusib	-4.86	272.24	ASN186	PHE67, LYS183, CYS199, ILE62, VAL110, ALA83, LEU188

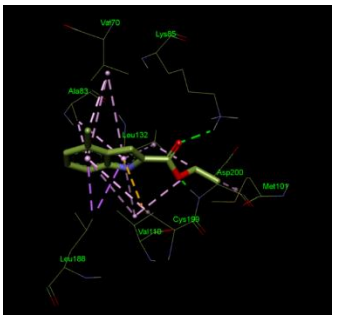

Figure No. 3a displaying Ligand Ai1- The carbonyl oxygen (in red) is seen involved in a hydrogen donor-acceptor relationship (shown in green colour) with one of the amino hydrogens (displayed in blue and white) on the side chain of Lys85. Side chain of Leu188, Val110 and Val70 involved in hydrophobic interaction (purple broken lines) with the π electron cloud of indole nucleus.

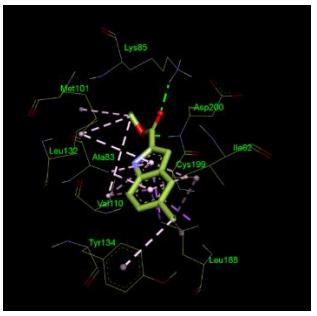

Figure No. 3b: Ligand Aii1- The carbonyl oxygen (in red) is seen involved in hydrogen donor-acceptor relationship (shown in green colour) with one of the amino hydrogens (displayed in blue and white) on the side chain of Lys85. Whereas, the lone pair electrons in 4-Chloro group is seen involved in hydrophobic

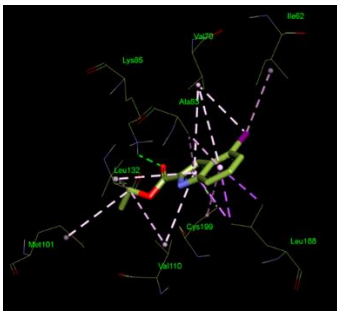

Figure No. 3c: Ligand Ai4- The carbonyl oxygen (in red) is seen involved in hydrogen donor-acceptor relationship (shown in green colour) with one of the amino hydrogens (displayed in blue and white) on the side chain of Lys85. Side chain of Ala83, Val110, Cys199, Leu132 and Leu188 involved in hydrophobic interaction (purple broken lines) with the π electron cloud of indole

interaction with the nucleus. π electron cloud of Tyr134.

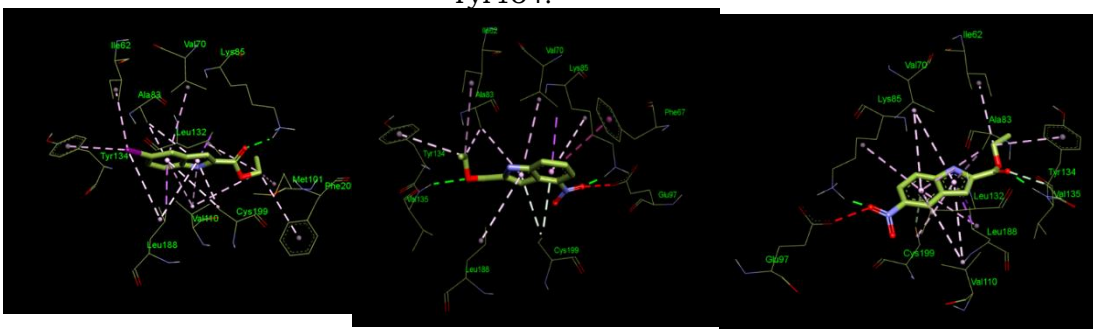

Figure No. 3d: Ligand Aii4- The carbonyl oxygen (in red) is seen involved in hydrogen donor-acceptor relationship (shown in green colour) with one of the amino hydrogens (displayed in blue and white) on the side chain of Lys85. Side chain of Leu188, Val110, Phe201, Ala83 and Val70 involved in hydrophobic interaction (purple broken lines) with the π electron cloud of indole nucleus.

Figure No. 3.e: Ligand Ai5- The carbonyl oxygen (in red) is seen involved in hydrogen donor-acceptor relationship (shown in green colour) with one of the amino hydrogens (displayed in blue and white) on the side chain of Val135. Whereas, oxygen of 4-nitro group is seen involved in hydrophilic interaction with the side chain of Lys88

Figure No. 3f: Ligand Aii5- The carbonyl oxygen (in red) is seen involved in hydrogen donor-acceptor relationship (shown in green colour) with one of the amino hydrogens (displayed in blue and white) on the side chain of Val135. Side chain of Ala83, Val110, Cys199, Leu132 and Leu188 involved in hydrophobic interaction (purple broken lines) with the π electron cloud of indole nucleus.

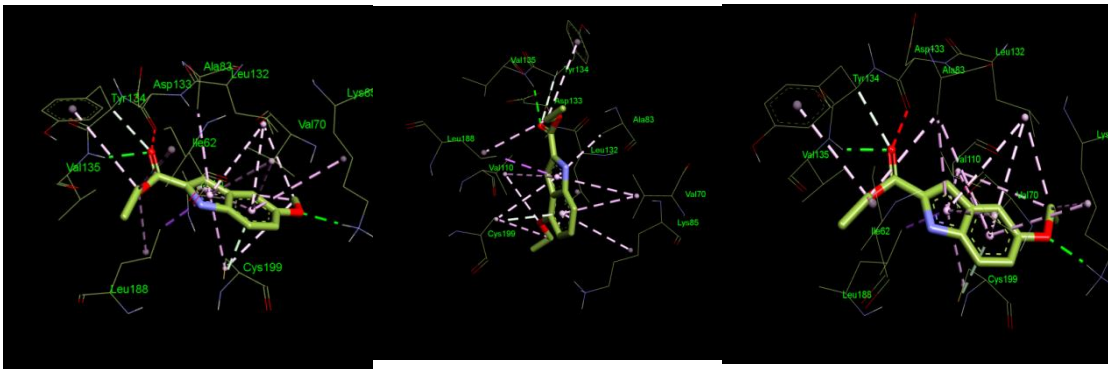

Figure No. 3g: Ligand Aii6- The carbonyl oxygen (in red) is seen involved in

Figure No. 3h: Ligand Ai10- The carbonyl oxygen (in red) is seen

Figure No. 3i: Ligand Aii10- The carbonyl oxygen (in red) is seen involved in

hydrogen donor-acceptor relationship (shown in green colour) with one of the amino hydrogens (displayed in blue and white) on the side chain of Val135. Whereas, oxygen of 5-methoxy group is seen involved in hydrophilic interaction with the side chain of Lys85.

involved in hydrogen donor-acceptor relationship (shown in green colour) with one of the amino hydrogens (displayed in blue and white) on the side chain of Val135. Side chain of Ala83, Val110, Cys199, Leu132 and Leu188 involved in hydrophobic interaction (purple broken lines) with the π electron cloud of indole nucleus.

hydrogen donor-acceptor relationship (shown in green colour) with one of the amino hydrogens (displayed in blue and white) on the side chain of Val135. Whereas, oxygen of 5-ethoxy group is seen involved in hydrophilic interaction with the side chain of Lys85.

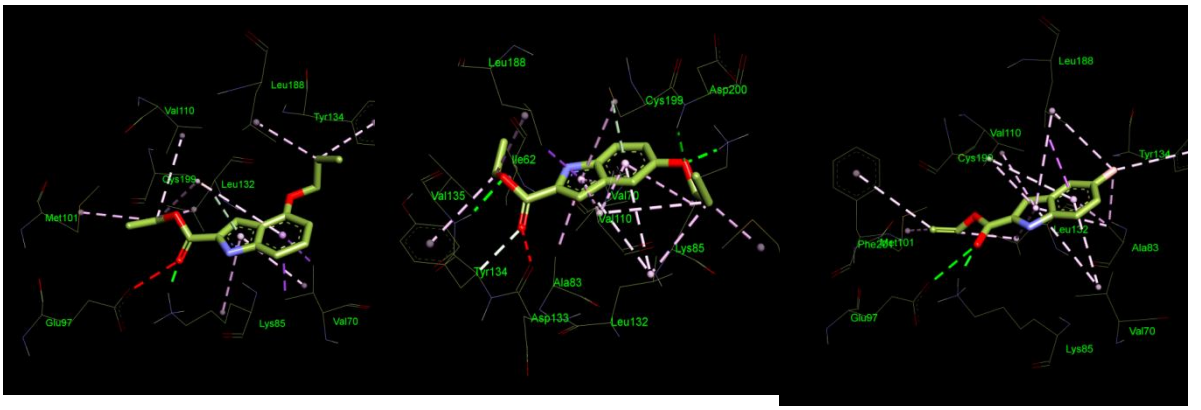

Figure No. 3j: Ligand Ai11- The carbonyl oxygen (in red) is seen involved in hydrogen donor-acceptor relationship (shown in green colour) with one of the amino hydrogens (displayed in blue and white) on the side chain of Lys85. Side chain of Val70, Cys199 involved in hydrophobic interaction (purple broken lines) with the π electron cloud of indole nucleus.

Figure No. 3k: Ligand Aii11- Oxygen (in red) of propyl side chain is seen involved in hydrogen donor-acceptor relationship (shown in green colour) with one of the amino hydrogens (displayed in blue and white) on the side chain of Asp200 and Cys199. Side chain of Ala83, Val110, Lys85, and Leu188 involved in hydrophobic interaction (purple broken lines) with the π electron cloud of indole nucleus.

Figure No. 3l: Ligand Aii2- The carbonyl oxygen (in red) is seen involved in hydrogen donor-acceptor relationship (shown in green colour) with one of the amino hydrogens (displayed in blue and white) on the side chain of Lys85 and with aromatic ring of Glu97. Side chain of Ala83, Val70, Cys199, and Val110 involved in hydrophobic interaction (purple broken lines) with the π electron cloud of indole nucleus.

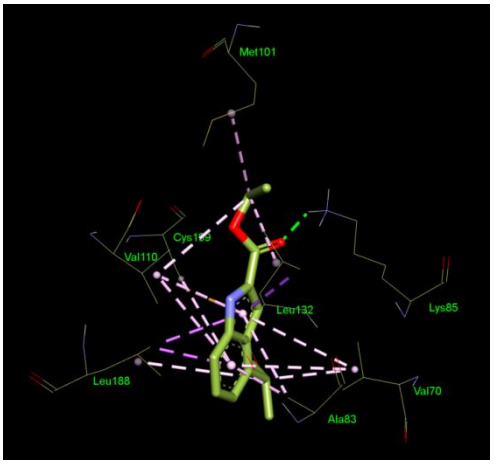

Figure No. 3m: Ligand Ai12- The carbonyl oxygen (in red) is seen involved in hydrogen donor-acceptor relationship (shown in green colour) with one of the amino hydrogens (displayed in blue and white) on the side chain of Lys85. Side chain of Ala83, Val110, Cys199 and Leu132 involved in hydrophobic interaction (purple broken lines) with the π electron cloud of indole nucleus.

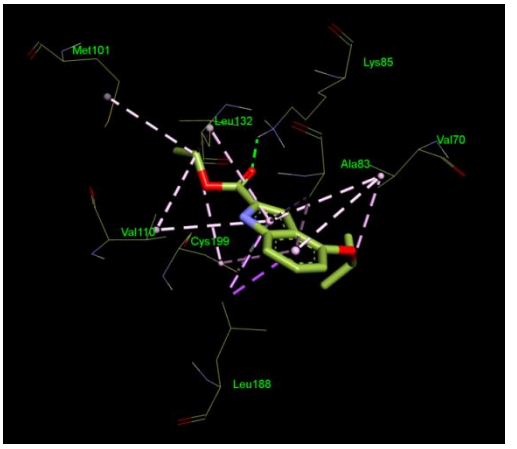

Figure No. 3n: Ligand Aii13- The carbonyl oxygen (in red) is seen involved in hydrogen donor-acceptor relationship (shown in green colour) with one of the amino hydrogens (displayed in blue and white) on the side chain of Val135. Side chain of Ala83, Val110, Cys199, Leu132 and Leu188 involved in hydrophobic interaction (purple broken lines) with the π electron cloud of indole nucleus.

Figure No. 3 (3a-3n): The docking poses of Substituted ethyl-1*H*-indole-2/3-carboxylate derivatives in the binding site of the *GSK-3β* in the complex (PDB ID: 6V6L)

ADME analysis

In silico analyses displayed few drug-like properties possessed by the designed ligands. The molecular weights of design ligands fall between 223 and 315 Daltons. The values of H bond Donor-Acceptor were found within acceptable range. The values of Log *P*, Log *S* molar refractivity, and total polar surface area (TPSA) predicted by the *SwissADME* predictor in these compounds were in excellent accord with the rule for most essential drug-likeness. Though these compounds exhibited a good hydrophilic–lipophilic balance demonstrating sufficient bioavailability, the -propoxy and -isopropyl (Ai11, Aii11, Ai12 and Ai13) derivatives with high lipophilicity are expected to show decent GI absorption. Passively absorbed molecules with TPSA of molecules ≥140 are thought to have low oral bioavailability [(25)], hence TPSA of the designed ligands were ranging 42.05 - 87.91. All designed ligands observed the *Lipinski Rule of Five* and PAINS alert. All the designed ligands show significate synthetic accessibility except Ai11, Aii11. The results obtained from the *SwissADME* search engine are listed in Table No. 5.

The Bioavailability Radar diagram, displayed in Figure No. 4 of these ligands show properties required for drug-likeness of a ligands. The pink area signify the

optimal range for each properties, as lipophilicity: Log *P* between -0.7 and + 5.0; size: MW between 150 and 500 g/mol; polarity: TPSA between 20 and 130 Å 2; solubility: Log *S* ≤ 6; saturation: fraction of carbons in the SP^3 hybridization ≥ 0.25, and flexibility: ≤ 9 rotatable bonds. The ligands; Ai1, Aii1, Aii2, Ai4, Aii4, Ai5 and Aii5 are predicted to be poorly bioavailable, because of too high percentage of saturation indicating them to be non-polar.

Ligand	Bioavailability radar graph	Ligand	Bioavailability radar graph
Ai1	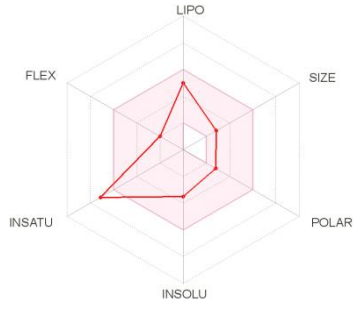	Aii6	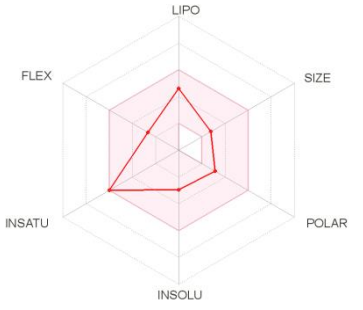
Aii1	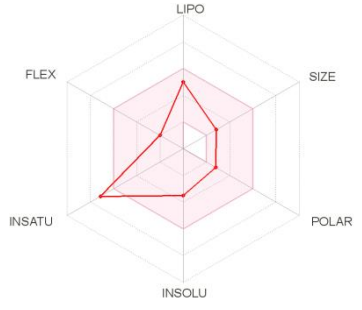	Ai10	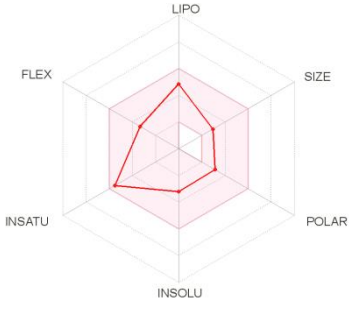
Aii2	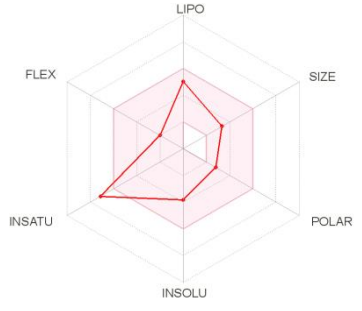	Aii10	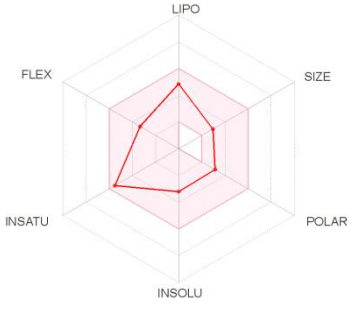

Ai4	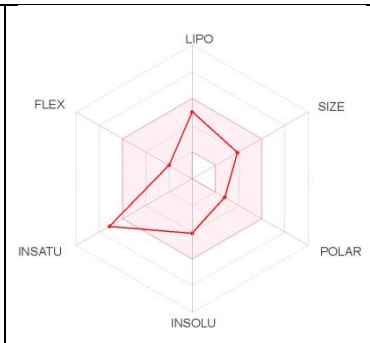	Ai11	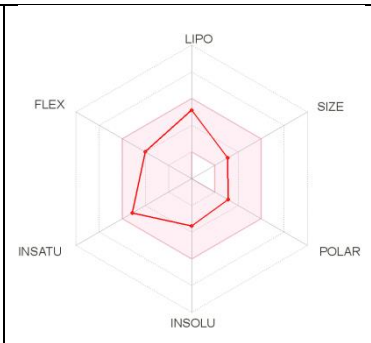
Aii4		Aii11	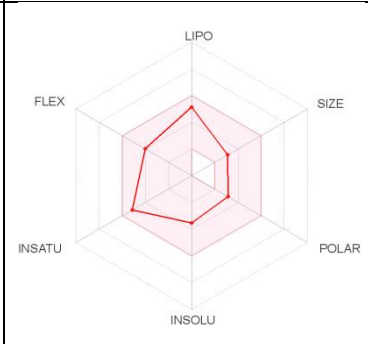
Ai5	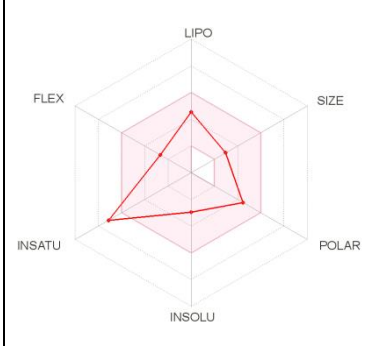	Ai12	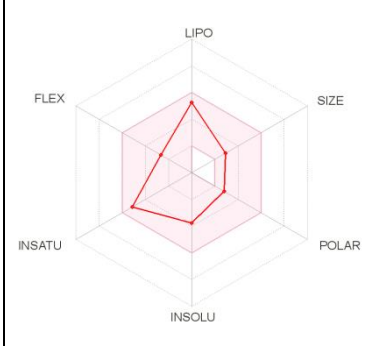
Aii5	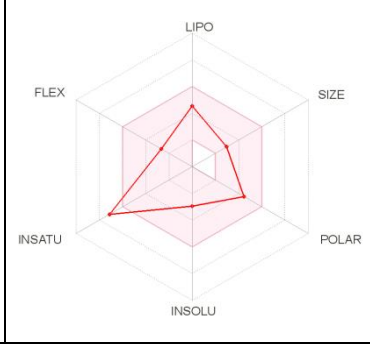	Ai13	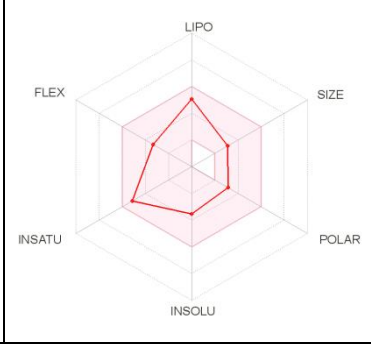

Figure 4. Bioavailability radar graph of Ethyl 2/3-carboxylate-4/5/6-monosubstituted-1H-indole derivative (pink area reflects the allowed values of drug likeness properties of the molecule)

Table 5
Physicochemical descriptors and ADME parameters

Ligand	MW	R Bond	HA	HD	TPSA	MR	W log P (lipophilicity)	ESOL log S	GI absorption	BBB permeant	log Kp (cm/s)	Lipinski violations	Synthetic accessibility
Ai1	223.66	3	2	1	42.09	59.4	3	-3.51	High	YES	-5.37	0	1.87
Aii1	223.66	3	2	1	42.09	59.4	3	-3.51	High	YES	-5.37	0	1.83
Aii2	268.11	3	2	1	42.09	62.09	3.11	-3.82	High	Yes	-5.6	0	1.86
Ai4	315.11	3	2	1	42.09	67.1	2.95	-4.09	High	Yes	-5.91	0	2.23
Aii4	315.11	3	2	1	42.09	67.1	2.95	-4.09	High	Yes	-5.91	0	2.09
Ai5	234.21	4	4	1	87.91	63.61	2.25	-2.95	High	Yes	-6	0	2.12
Aii5	234.21	4	4	1	87.91	63.61	2.25	-2.95	High	Yes	-6	0	2.21
Aii6	219.24	4	3	1	51.32	60.88	2.35	-2.97	High	Yes	-5.81	0	1.86
Ai10	233.26	5	3	1	51.32	65.68	2.94	-3.2	High	Yes	-5.64	0	2.09
Aii10	233.26	5	3	1	51.32	65.68	2.94	-3.2	High	Yes	-5.64	0	2.01
Ai11	247.29	6	3	1	51.32	70.49	3.13	-3.53	High	Yes	-5.34	0	0.55
Aii11	247.29	6	3	1	51.32	70.49	3.13	-3.53	High	Yes	-5.34	0	0.55
Ai12	231.29	4	2	1	42.09	68.97	3.47	-3.75	High	Yes	-5.06	0	2.11
Ai13	247.29	5	3	1	51.32	70.49	3.13	-3.54	High	Yes	-5.42	0	2.18

(R bond = rotatable bond; H-A = hydrogen bond-acceptor; H-D = hydrogen bond-donor; MR = molar refractivity; TPSA = topological polar surface area; Log *P* = lipophilicity; Log *S* = water solubility; Log *Kp* = permeability coefficient; PAINS = pan-assay interference structure)

Table 6
Toxicity profile of selected ligands

Ligand	*Algae at*	*Ames test*	*Carcino Mouse*	*Carcino Rat*	*Daphnia at*	*hERG inhibition*	*Medaka at*	*minnow at*
Ai1	0.035633	mutagen	positive	negative	0.0723432	medium risk	0.00853105	0.00929891
Aii1	0.0358677	mutagen	positive	negative	0.0698611	medium risk	0.00798963	0.00935652
Aii2	0.0327086	mutagen	positive	negative	0.055813	medium risk	0.0055078	0.00752524
Ai4	0.0357435	mutagen	positive	positive	0.0286209	medium risk	0.002156	0.00325565
Aii4	0.035979	mutagen	positive	positive	0.0277415	medium risk	0.00203327	0.00327582
Ai5	0.0677396	mutagen	negative	positive	0.1221016	medium risk	0.0226102	0.0180484
Aii5	0.0668478	mutagen	negative	positive	0.184708	medium risk	0.0500255	0.0181402
Aii6	0.0527986	mutagen	positive	negative	0.159006	medium risk	0.036926	0.0317204
Ai10	0.0421856	mutagen	negative	negative	0.12225	medium	0.024014	0.0181488

						risk		
Aii10	0.0407121	mutagen	positive	negative	0.121853	medium risk	0.0222648	0.0182345
Ai11	0.029477	mutagen	negative	negative	0.0873315	medium risk	0.011722	0.00748428
Aii11	0.0282851	mutagen	positive	negative	0.0780311	medium risk	0.00948769	0.00752157
Ai12	0.0260728	mutagen	positive	negative	0.0473085	medium risk	0.00359663	0.00529715
Ai13	0.0322471	mutagen	negative	negative	0.0922252	medium risk	0.0130973	0.00967045

Another provision in *SwissADME* is to predict the distribution of designed ligands in different compartment in body [32], and displays the result in a *Boiled-egg diagram* shown below (Figure No. 05). According to this analysis, ligands Ai12, Aii11, Aii1, Aii2, Aii4, Ai1, Ai4, Ai11, Ai13, Ai10 Aii10, Aii6 shown in the yellow portion pass the blood–brain barrier (BBB), whereas Ai5 and Aii5 are present in the white area can be absorbed very easily by the gastrointestinal tract.

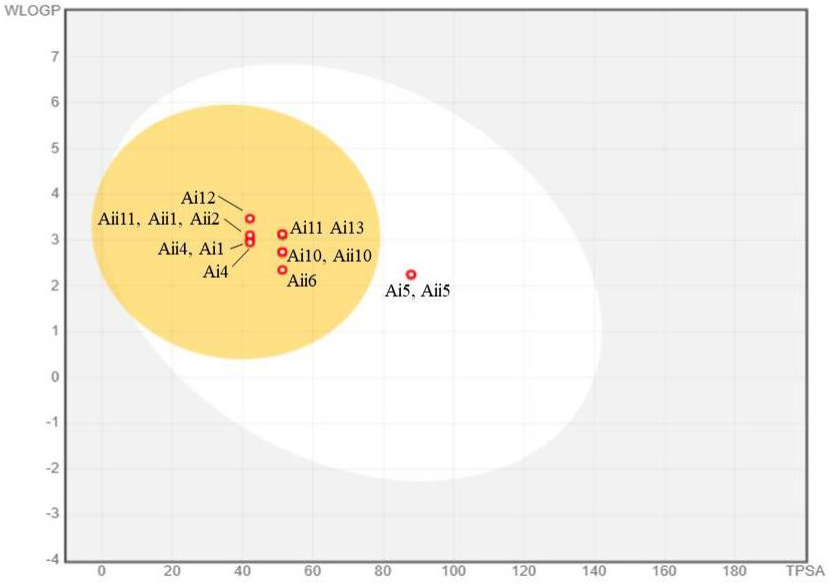

Figure 5. ADME properties of Ligands by graphical representation (boiled-egg) (predict gastrointestinal absorption and brain penetration of small molecules) Yellow color indicates BBB, White color indicates gastrointestinal track

Conclusion

Designed ligands, 906 Ethyl 2/3-carboxylate-4/5/6-monosubstituted-1*H*-indole derivatives, were subjected to molecular docking, *in silico* ADME, toxicity profile studies, and were eventually tapered to 12 based on acceptable *G-score* and ligand-protein interactions, favourable properties to fit in *The Lipinski rule of five*. Results analysis suggested that the compounds are promising leads for the discovery of potential *GSK-3β* enzyme inhibitor. Ligands with - *chloro,* - *nitro* and - *alkyl* substitution at 4, 5, 6, 7 positions show significant binding energy and docking score. These 12 compounds need to be synthesized and evaluated for

their potential to inhibit *GSK-3β*. The present article stands on a purely computational approach using the best possible utilities available.

Conflicts of interest

The authors declare that there are no conflicts of interest in the studies leading to this manuscript.

Acknowledgements

Authors are thankful to Shriman Sureshdada Jain College of Pharmacy, Chandwad, for providing necessary facilities to accomplish the present work. Words of gratitude are also due for GES's Sir Dr. M. S. Gosavi College Pharmaceutical Education and Research, Nashik.

List of Abbreviations

LBD: Ligand binding domain
ADMET: absorption, distribution
GSK-3β: Glycogen Synthase Kinase
GS: Glycogen Synthase
ADT: Auto Dock Tools
R bond: rotatable bond
RMSD: root mean square deviation
H-A: hydrogen bond-acceptor
H-D: hydrogen bond-donor; MR = molar refractivity
TPSA: topological polar surface area
Log *P*: lipophilicity
Log *S*: water solubility
Log *Kp*: permeability coefficient
PAINS: pan-assay interference structure

References

1. Renfrey S, Featherstone J. Structural proteomics. Nature Reviews. Drug Discovery. 2002 Mar 1; 1 (3):175. DOI: 10.1038/nrd766.
2. Frame S, Cohen P. *GSK-3* takes center stage more than 20 years after its discovery. Biochemical Journal. 2001 Oct 1; 359 (1):1-6. DOI: 10.1042/0264-6021:3590001.
3. Doble BW, Woodgett JR. *GSK-3*: tricks of the trade for a multi-tasking kinase. Journal of Cell Science. 2003 Apr 1; 116 (7):1175-86. DOI: 10.1242/jcs.00384.
4. Jope RS, Johnson GV. The glamour and gloom of *glycogen synthase kinase-3*. Trends in Biochemical Sciences. 2004 Feb 1; 29 (2):95-102. DOI: 10.1016/j.tibs.2003.12.004.
5. Grimes CA, Jope RS. The multifaceted roles of *glycogen synthase kinase 3β* in cellular signaling. Progress in Neurobiology. 2001 Nov 1; 65 (4):391-426. DOI:10.1016/S0301-0082(01)00011-9.

6. Eldar-Finkelman H. *Glycogen synthase kinase 3*: an emerging therapeutic target. Trends in Molecular Medicine. 2002 Mar 1; 8 (3):126-32. DOI: 10.1016/s1471-4914(01)02266-3.
7. Ilouz R, Kaidanovich O. Gurwitz D, et al. Inhibition of *glycogen synthase kinase-3β* by bivalent zinc ions: insight into the insulin-mimetic action of zinc. Biochemical and Biophysical Research Communications. 2002 Jul 5; 295 (1):102-6. DOI: 10.1016/s0006-291x(02)00636-8.
8. Meijer L, Thunnissen AM, White AW, et al. Inhibition of cyclin-dependent kinases, *GSK-3β* and CK1 by hymenialdisine, a marine sponge constituent. Chemistry & Biology. 2000 Jan 1; 7(1):51-63. DOI: 10.1016/s1074-5521(00)00063-6.
9. Castro A, Martinez A. Inhibition of tau phosphorylation: a new therapeutic strategy for the treatment of Alzheimer's disease and other neurodegenerative disorders. Expert Opinion on Therapeutic Patents. 2000 Oct 1; 10 (10): 1519-27. DOI:10.1517/13543776.10.10.1519.
10. Zhang F, Phiel CJ, Spece L, et al. Inhibitory phosphorylation of *glycogen synthase kinase-3 (GSK-3)* in response to lithium: evidence for autoregulation of GSK-3. Journal of Biological Chemistry. 2003 Aug 29; 278 (35): 33067-77. DOI:10.1074/jbc.M212635200.
11. Leost M, Schultz C, Link A, et al. Paullones are potent inhibitors of glycogen synthase kinase-3β and cyclin-dependent kinase 5/p25. European Journal of Biochemistry. 2000 Oct; 267 (19):5983-94. PMID10998059.
12. Meijer L, Skaltsounis AL, Magiatis P, et al. *GSK-3*-selective inhibitors derived from Tyrian purple indirubins. Chemistry & Biology. 2003 Dec 1; 10 (12):1255-66. DOI: 10.1016/j.chembiol.2003.11.010.
13. Dessalew N, Bharatam PV. Structure based de novo design of novel *glycogen synthase kinase 3* inhibitors. Bioorganic & Medicinal Chemistry. 2007 Jun 1; 15 (11):3728-36. DOI: 10.1016/j.bmc.2007.03.048.
14. David GS, Marianne B, Ashley EF, et al, Robert WW. 3-Anilino-4-arylmaleimides: potent and selective inhibitors of *glycogen synthase kinase-3.* Bioorganic & Medicinal Chemistry Letters. 200; 11: 635-9. DOI: 10.1016/S0960-894X(00)00721-6.
15. Crisan L, Avram S, Bora A, Kurunczi L, et al., 3D-QSAR study of maleimide analogues as *glycogen synthase kinase-3 (gsk-3)* inhibitors using comsia approach. Revue Roumaine de Chimie. 2015 Feb 1; 60 (2-3):183-8.
16. Faulds KJ, Egelston JN, Sedivy LJ, et al. *Glycogen synthase kinase-3 (GSK-3)* activity regulates mRNA methylation in mouse embryonic stem cells. Journal of Biological Chemistry. 2018 Jul 6; 293 (27):10731-43. DOI: 10.1074/jbc.ra117.001298
17. Walters WP, Murcko MA. Prediction of 'drug-likeness'. Advanced Drug Delivery Reviews. 2002 Mar 31; 54 (3):255-71. DOI: 10.1016/S0169-409X(02)00003-0.
18. Hollingsworth SA, Karplus PA. A fresh look at the Ramachandran plot and the occurrence of standard structures in proteins. BioMolecular Concepts 1(1); 2010, 271–283. DOI:10.1515/bmc.2010.022.
19. Zhou AQ, O'Hern CS, Regan L. Revisiting the Ramachandran plot from a new angle. Protein Science. 2011 Jul; 20 (7): 1166-71. DOI: 10.1002/pro.644.
20. Nisha CM, Kumar A, Vimal A, et al. Docking and ADMET prediction of few *GSK-3* inhibitors divulges 6-bromoindirubin-3-oxime as a potential inhibitor.

Journal of Molecular Graphics and Modelling. 2016 Apr 1; 65: 100-7. https://doi.org/10.1016/j.jmgm.2016.03.001.
21. Trott O, Olson AJ. AutoDock Vina: improving the speed and accuracy of docking with a new scoring function, efficient optimization, and multithreading. Journal of Computational Chemistry. 2010 Jan 30; 31 (2):455-61. DOI: 10.1002/jcc.21334.
22. Rylander SG, Gotshall B. Optimal population size and the genetic algorithm. Population. 2002; 100 (400):900. Corpus ID: 15152896.
23. 1-(6-((2-((6-amino-5-nitropyridin-2-yl)amino)ethyl)amino)-2-(2,4-dichlorophenyl)pyridin-3-yl)-4-methylpiperazin-2-one
24. Lipinski CA, Lombardo F, Dominy BW, et al. Experimental and computational approaches to estimate solubility and permeability in drug discovery and development settings. Advanced Drug Delivery Reviews. 1997 Jan 15; 23 (1-3):3-25. DOI: 10.1016/s0169-409x(00)00129-0.
25. Veber DF, Johnson SR, Cheng HY, et al., Molecular properties that influence the oral bioavailability of drug candidates. Journal of Medicinal Chemistry. 2002 Jun 6; 45 (12):2615-23. DOI: 10.1021/jm020017n.
26. Daina A, Michielin O, Zoete V., SwissADME: a free web tool to evaluate pharmacokinetics, drug-likeness and medicinal chemistry friendliness of small molecules. Scientific Reports. 2017 Mar 3; 7 (1):1-3. DOI: 10.1038/srep42717.
27. Doak BC, Over B, Giordanetto F, et al. Oral druggable space beyond the rule of 5: insights from drugs and clinical candidates. Chemistry & Biology. 2014 Sep 18; 21 (9):1115-42. DOI: 10.1016/j.chembiol.2014.08.013.
28. Moroy G, Martiny VY, Vayer P, et al. Toward in silico structure-based ADMET prediction in drug discovery. Drug Discovery Today. 2012 Jan 1; 17 (1-2):44-55. DOI: 10.1016/j.drudis.2011.10.023.
29. Martinez A, Castro A, Dorronsoro I et al. *Glycogen synthase kinase 3 (GSK-3)* inhibitors as new promising drugs for diabetes, neurodegeneration, cancer, and inflammation. Medicinal Research Reviews. 2002 Jul; 22(4):373-84. DOI: 10.1002/med.10011.
30. Meijer L, Flajolet M, Greengard P. Pharmacological inhibitors of *glycogen synthase kinase 3*. Trends in Pharmacological Sciences. 2004 Sep; 25(9):471-80. DOI: 10.1016/j.tips.2004.07.006.
31. Lo Monte F, Kramer T, Gu J, et al, Plotkin B, Eldar-Finkelman H, Schmidt B. Identification of *glycogen synthase kinase-3* inhibitors with a selective sting for *glycogen synthase kinase-3a.* Journal of Medicinal Chemistry. 2012 May 10; 55 (9):4407-24. DOI: 10.1021/jm300309a
32. Medina M, Castro A. *Glycogen synthase kinase-3 (GSK-3)* inhibitors reach the clinic. Current Opinion in Drug Discovery & Development. 2008 Jul; 11 (4):533-43. DOI: 10.7150/thno.14334
33. Daina A, Zoete V. A boiled-egg to predict gastrointestinal absorption and brain penetration of small molecules. ChemMedChem. 2016 Jun 6; 11 (11):1117. DOI: 10.1002/cmdc.201600182
34. Rinartha, K., Suryasa, W., & Kartika, L. G. S. (2018). Comparative Analysis of String Similarity on Dynamic Query Suggestions. In 2018 Electrical Power, Electronics, Communications, Controls and Informatics Seminar (EECCIS) (pp. 399-404). IEEE.

35. Suryasa, I. W., Rodríguez-Gámez, M., & Koldoris, T. (2021). Get vaccinated when it is your turn and follow the local guidelines. International Journal of Health Sciences, 5(3), x-xv. https://doi.org/10.53730/ijhs.v5n3.2938
36. Mahardika, I. M. R., Suyasa, I. G. P. D., Kamaryati, N. P., & Wulandari, S. K. (2021). Health literacy is strongest determinant on self-monitoring blood glucose (SMBG) type 2 DM patients during COVID-19 pandemic at public health centre in Tabanan Regency. International Journal of Health & Medical Sciences, 4(3), 288-297. https://doi.org/10.31295/ijhms.v4n3.1752